



Cite this: RSC Adv., 2017, 7, 50234

 Received 5th September 2017
 Accepted 21st October 2017

 DOI: 10.1039/c7ra09872c
rsc.li/rsc-advances

Near-infrared optical performances of two Bi_2Se_3 nanosheets[†]

 Hanhan Xie,^a Jundong Shao,^b Jiahong Wang,^{*b} Zhengbo Sun,^b Xue-Feng Yu^{id *b} and Qu-Quan Wang^{id *a}

Bi_2Se_3 has been widely used as a promising photothermal and photoacoustic agent recently. Herein, two-dimensional (2D) Bi_2Se_3 nanosheets with different sizes of about 30 nm (Bi_2Se_3 -30) and 80 nm (Bi_2Se_3 -80) have been successfully synthesized via solution-based methods. Both of the Bi_2Se_3 nanosheets possess high near-infrared (NIR) optical absorption, efficient photothermal conversion and excellent photoacoustic behaviors. Meanwhile, the Bi_2Se_3 -30 nanosheets perform better. These results indicate the smaller Bi_2Se_3 nanosheets are more promising for optical diagnostic and photothermal therapy.

1. Introduction

As new quantum matter, topological insulators are one of the most exciting research topics in physics, chemistry and materials fields.^{1,2} In recent years, great efforts have been devoted to theoretical prediction and experimental confirmation of various 2D topological insulators such as Bi_2Se_3 , Bi_2Te_3 , Sb_2Te_3 etc.³⁻⁷ Among them, Bi_2Se_3 invokes a research boom due to its simple band structure near the Dirac point and remarkable band gap.³⁻⁵ The unique band structure of Bi_2Se_3 lead to new electronic and optical properties.^{8,9} For instance, owing to its graphene-like Dirac energy band structure in its surface state, Bi_2Se_3 can operate as a broadband optical material possess remarkable NIR absorption capacity. Furthermore, Bi_2Se_3 nanosheets exhibit good bioactivity, biocompatibility, and metabolizability, thus have been proposed as a novel NIR optical nanoagent for bioimaging and therapy applications.¹⁰⁻¹³ Their advantageous 2D structure is also promising for many other biomedical applications such as drug delivery.¹⁴

It is known that the size of the quantum materials is critically important to their chemical, physical and biological properties. For 2D Bi_2Se_3 , the decrease of diameter or thickness can enlarge the energy gap,¹⁵ enhance the electron-phonon coupling,¹⁶ and regulate the optical properties.⁹ On the other hand, the size of Bi_2Se_3 is also crucial when used as a nanoagent in biomedical applications, which influences not only its cell uptake and biocompatibility,¹⁷ but also its *in vivo* clearance.¹⁸ Recently, many

research groups including ours have established polyol synthesis strategies to prepare Bi_2Se_3 nanosheets and investigate their optical properties.^{13,19-23} However, the size effect on the optical properties of Bi_2Se_3 nanosheets has not been reported.

In this study, two Bi_2Se_3 nanosheets with well-controlled particle sizes of 30 nm and 80 nm are synthesized and their optical absorption properties, NIR photothermal and photoacoustic performances are systematically investigated.

2. Experimental section

2.1. Materials

The materials used in this study, selenium powders (Se, 99.0%), acetone ($\geq 99.8\%$) and ethylene glycol (EG, $\geq 99.0\%$) were obtained from Sinopharm Chemical Reagent Co. Ltd. (Shanghai, China). Sodium borohydride (NaBH_4 , 96.0%), bismuth nitrate pentahydrate ($\text{Bi}(\text{NO}_3)_3 \cdot 5\text{H}_2\text{O}$, 99.99%+), poly(vinylpyrrolidone) (PVP, MW \approx 55 000), sodium selenite (Na_2SeO_3 , 99.0%), and hydroxylamine (NH_2OH) were purchased from Sigma-Aldrich. Ultrapure water ($18.25\text{ M}\Omega\text{ cm}$, 25 °C) was used in the experiments.

2.2. Synthesis of Bi_2Se_3 -30 nanosheets

The Bi_2Se_3 -30 nanosheets were synthesized following our previously reported method.²⁰ Firstly, the sodium hydrogen selenium (NaHSe) solution was pre-produced by the reaction of NaBH_4 aqueous solution and Se powders in an ice-water bath. Then, 0.5 g $\text{Bi}(\text{NO}_3)_3 \cdot 5\text{H}_2\text{O}$ and 0.226 g PVP were mixed at room temperature in ethylene glycol (EG). The well-mixed transparent solution turned turbid yellow when heated to 160 °C under a nitrogen environment. The pre-prepared oxygen-free NaHSe solution (0.667 mol L^{-1} , 1.048 mL) was rapidly injected into the mixture by a syringe. The mixture turned dark immediately, indicating the formation of Bi_2Se_3 -30 nanosheets. The reaction was continued 10 min before cooling to room temperature.

^aDepartment of Physics, Key Laboratory of Artificial Micro- and Nano-structures of Ministry of Education, School of Physics and Technology, Wuhan University, Wuhan 430072, China. E-mail: qqwang@whu.edu.cn

^bInstitute of Biomedicine and Biotechnology, Shenzhen Institutes of Advanced Technology, Chinese Academy of Sciences, Shenzhen 518055, P. R. China. E-mail: xf.yu@siat.ac.cn; jh.wang1@siat.ac.cn

† Electronic supplementary information (ESI) available. See DOI: [10.1039/c7ra09872c](https://doi.org/10.1039/c7ra09872c)



2.3. Synthesis of Bi_2Se_3 -80 nanosheets

The Bi_2Se_3 -80 nanosheets were synthesized as previously published.¹⁹ 1.0 g PVP was dissolved in 50 mL EG, then poured into 250 mL round-bottom flask, followed by the addition of a solution of Na_2SeO_3 (0.242 g in 35 mL of EG) and $\text{Bi}(\text{NO}_3)_3 \cdot 5\text{H}_2\text{O}$ (0.452 g in 25 mL of EG) under magnetic stirring at room temperature. The sealed flask was heated to 160 °C under a nitrogen environment. The reaction took place by rapid injection of a hydroxylamine solution (NH_2OH , 2.4 mL in 20 mL of EG). The reaction mixture turned dark purple immediately, indicating the formation of Bi_2Se_3 -80 nanosheets. The reaction was continued 10 min for a complete reaction before cooling to room temperature.

2.4. Characterizations

Transmission electron microscopy (TEM) and high-resolution TEM (HR-TEM) images were acquired on the Tecnai G2 F20 S-Twin transmission electron microscope at an acceleration voltage of 200 kV. Powder X-ray diffraction (XRD) patterns were obtained on the D8 Advance (Bruker, Germany) with $\text{Cu K}\alpha$ radiation ($\lambda = 0.1542 \text{ nm}$) at 40 kV and 40 mA. Energy-dispersive X-ray spectrometry (EDS) was performed on the SEM equipped with an Oxford INCA 300. Atomic force microscopy (AFM) images were obtained from the MFP-3D-S atomic force microscope (Asylum Research, USA) using the AC mode (tapping mode) in the air. The UV-vis-NIR extinction spectra were recorded on a Lambda25 spectrophotometer (PerkinElmer) with QS-grade quartz cuvettes at room temperature. The Bi_2Se_3 concentrations were measured by an inductively-coupled plasma optical emission spectrometry (ICP-OES, 7000DV, PerkinElmer).

2.5. NIR photothermal effect measurement

The NIR photothermal effect was determined with an infrared thermal imaging camera (Fluke Ti27, USA), using the fiber-coupled continuous semiconductor diode laser (808 nm, KS-810F-8000, Kai Site Electronic Technology Co., Ltd. Shanxi, China) as the irradiation source. All samples were dispersed in ultrapure water with the same absorbance intensities as 0.3 at 808 nm. Subsequently, a 1 cm path length quartz cuvette containing 1 mL of the corresponding sample was irradiated by the laser with a power density of 1.0 W cm^{-2} for 12 min. The laser spot was adjusted to cover the entire surface of the sample. The temperature during the heating and cooling periods was recorded one time per 30 s by the infrared thermal imaging camera.

2.6. Photoacoustic performance

The Bi_2Se_3 nanosheets aqueous solutions were placed in a hemispherical acrylic holder and suspended in the center of the imaging dimple of the Endra Nexus 128 photoacoustic instrument. The transducers were coupled to the sample plane by filling the bowl with water and maintained at 38 °C by a pumping system. The photoacoustic signals were obtained at an incident laser wavelength of 808 nm. The photoacoustic signal intensities were acquired by using the ROI in the baseline image and the intensity changes in the ROI of the sample images were calculated.

3. Results and discussion

3.1. Synthesis and characterizations of Bi_2Se_3 nanosheets

The two kinds of Bi_2Se_3 nanosheets were synthesized by solution-based methods illustrated in Experimental section. The morphologies of these Bi_2Se_3 nanosheets were characterized by TEM and HR-TEM (Fig. 1). The TEM images in Fig. 1a and b reveal the uniform morphologies of these two Bi_2Se_3 nanosheets. According to the statistical TEM analysis of 200 nanosheets, the average lateral sizes of the two Bi_2Se_3 nanosheets are determined to be approximately $30 \pm 5 \text{ nm}$ (denoted as Bi_2Se_3 -30) and $80 \pm 15 \text{ nm}$ (denoted as Bi_2Se_3 -80), respectively. Different from the smooth surface of the Bi_2Se_3 -30 nanosheets (Fig. 1c), a screw protrusion is observed in the center of the Bi_2Se_3 -80 nanosheets (Fig. 1e). The morphological differences may be attributed to the supersaturation of the reaction system.²⁴ However, the lattice fringes in Fig. 1d and f are both ascribed to the (110) plane of Bi_2Se_3 as 0.21 nm, which suggest similar crystalline structures between the two Bi_2Se_3 nanosheets.¹³ Additionally, the XRD analyses confirm the rhombohedral structure of the two Bi_2Se_3 nanosheets (JCPDS card no. 33-0214) (Fig. S1†).²⁵ The chemical compositions of them were further determined by EDS. It is confirmed that their ratios of Bi to Se both are 2 : 3 (Fig. S2†).

The AFM images in Fig. 2 show the 3D topographic morphologies of the Bi_2Se_3 -30 and Bi_2Se_3 -80 nanosheets, the corresponding thicknesses are determined by the cross-sectional analysis. The average thickness of the Bi_2Se_3 -30 nanosheets measured in the AFM image is statistically $1.8 \pm 0.5 \text{ nm}$ (Fig. 2b), which is as thin as two quintuple atomic layers of Bi_2Se_3 . Comparatively, the average thickness of the Bi_2Se_3 -80 nanosheets is $8.3 \pm 1.0 \text{ nm}$ (Fig. 2d), corresponding to a stack of 8 ± 1 quintuple layers.

3.2. Optical absorption properties

The absorption properties of the two Bi_2Se_3 nanosheets are further investigated. As shown in Fig. 3, the aqueous solution of the two Bi_2Se_3 nanosheets exhibit obvious absorption ranging

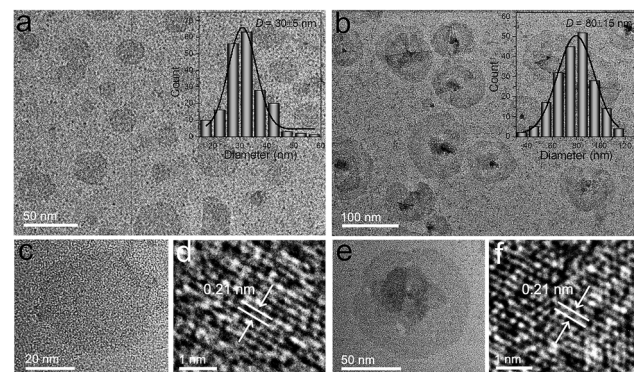


Fig. 1 TEM images of (a) Bi_2Se_3 -30 and (b) Bi_2Se_3 -80 nanosheets. Insets: diameter statistical graphs determined from the TEM images; (c) magnified TEM and (d) HR-TEM images of Bi_2Se_3 -30 nanosheets; (e) magnified TEM and (f) HR-TEM images of Bi_2Se_3 -80 nanosheets.



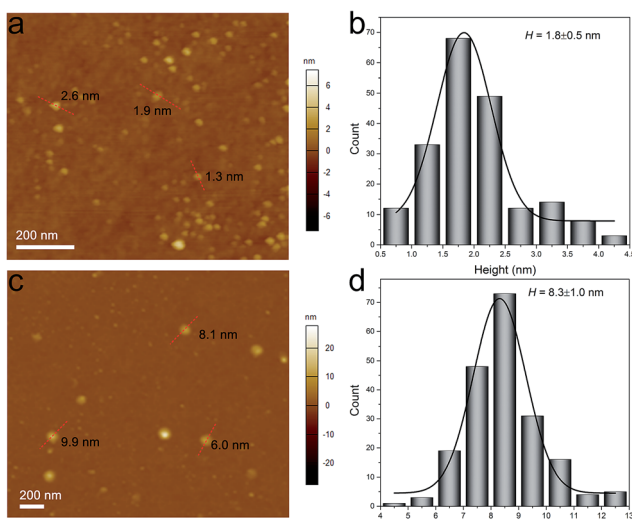


Fig. 2 AFM images and height statistical analysis of (a, b) Bi_2Se_3 -30 and (c, d) Bi_2Se_3 -80 nanosheets.

from ultraviolet to NIR, which is similar to other 2D layered materials such as graphene oxide²⁶ and black phosphorus.²⁷

Since the nanosheets concentrations (C) are measured by ICP-OES, and the extinction intensities against the quartz cell length (A/L) at $\lambda = 808$ nm are determined, the corresponding extinction coefficient ε can be obtained by using Beer's law: $A/L = \varepsilon C$. The extinction coefficients of Bi_2Se_3 -30 and Bi_2Se_3 -80 nanosheets at 808 nm are determined to be 11.3 and 10.7 $\text{L g}^{-1} \text{cm}^{-1}$, respectively. Both values are noticeably higher than the common photothermal agent gold nanorods (GNRs) (3.9 $\text{L g}^{-1} \text{cm}^{-1}$).²⁸

The optical band gap (E_g) of the two Bi_2Se_3 nanosheets are also investigated. E_g can be determined by the equation: $(\alpha h\nu)^n = B(h\nu - E_g)$,²⁹ in which α is the absorption coefficient, $h\nu$ is photon energy, and B is a constant. Here $n = 2$ offers the best fit for the optical absorption data of Bi_2Se_3 .^{29–31} The plots of $(\alpha h\nu)^2$ versus $h\nu$ for the Bi_2Se_3 nanosheets are shown in Fig. S3.† The E_g of the two Bi_2Se_3 nanosheets are acquired by extrapolating the straight portion of the plot to intersect the energy axis. The E_g of the Bi_2Se_3 -30 and Bi_2Se_3 -80 nanosheets are determined to be 2.14 and 1.99 eV, respectively.

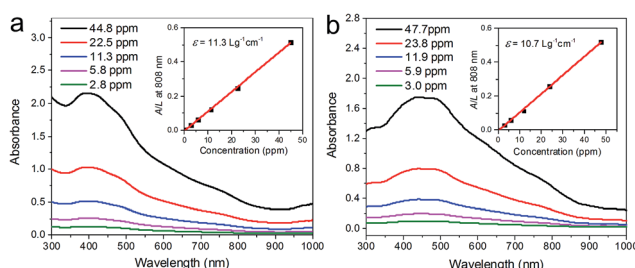


Fig. 3 Absorption spectra of (a) Bi_2Se_3 -30 and (b) Bi_2Se_3 -80 nanosheets with various concentrations. Insets: absorbance intensities against the quartz cell length (A/L) with different concentrations (C) at 808 nm.

3.3. Photothermal performance

The NIR photothermal performances of the two Bi_2Se_3 nanosheets were investigated by dispersing them in water with the same absorbance intensity of 0.30 at 808 nm. Then, the temperatures were measured during the irradiation of an 808 nm laser at low power density (1.0 W cm^{-2}) for 12 min.

The photographs and corresponding infrared thermal images of the solutions are shown in Fig. 4a, and their temperature heating and cooling curves are shown in Fig. 4b. Compared with pure water, the aqueous solutions of the two Bi_2Se_3 nanosheets show much more significant temperature increase. To further uncover the photothermal performance of the two Bi_2Se_3 nanosheets, the photothermal conversion efficiency (η) is calculated based on the energy balance of the system as shown below:^{32–34}

$$\eta = (hS(T_{\max} - T_{\text{surr}}) - Q_{\text{dis}})/I(1 - 10^{-A}) \quad (1)$$

$$hS = \sum mC_p/\tau_s \quad (2)$$

Where h is the heat transfer coefficient, S is the surface area of the container, T_{\max} is the maximum temperature at steady-state, T_{surr} is the surrounding ambient temperature, I is the laser power density (1.0 W cm^{-2}), and A is the absorption intensity at 808 nm ($A_{808} = 0.3$). Q_{dis} is the heat associated with light absorption by the solvent. The variable τ_s is the time constant for the heat transfer from the system, m and C_p are the mass (1.0 g) and the specific heat capacity (4.2 $\text{J g}^{-1} \text{C}^{-1}$) of the water used as the solvent. According to eqn (1) and (2), the η values of the Bi_2Se_3 -30 and Bi_2Se_3 -80 nanosheets are calculated to be 33% and 25%, respectively. The η value of the Bi_2Se_3 -30 nanosheets

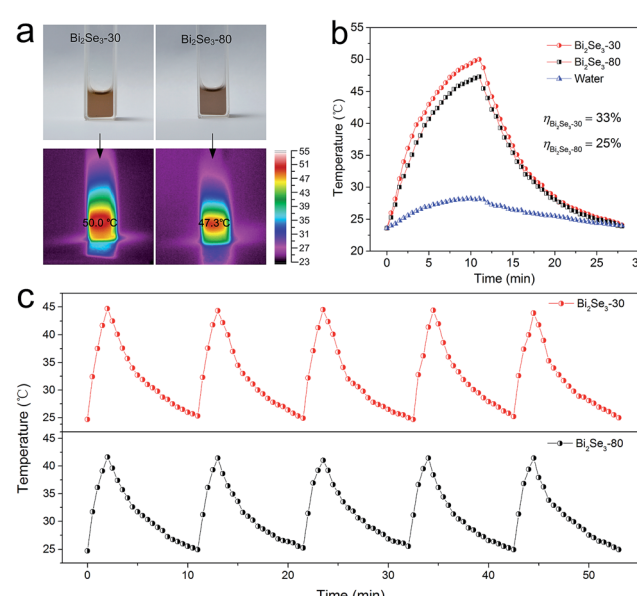


Fig. 4 (a) Photographs (top) and infrared thermal images (down) of the two Bi_2Se_3 nanosheets aqueous solution with the same absorption intensities of 0.3 at 808 nm. (b) Photothermal heating/cooling curves of the two Bi_2Se_3 nanosheets under 808 nm laser. (c) Temperature elevation of the two Bi_2Se_3 nanosheets for five laser on/off cycles.

is significantly higher than that of the Bi_2Se_3 -80 nanosheets. It could be a result of lower scattering introduced by the smaller particles, by which the external light can be efficiently absorbed instead of being scattered.³⁵ Additionally, the thinner structure usually performs more violent atomic oscillation, which is beneficial to the photothermal conversion.

To further evaluate the photothermal stability of the two Bi_2Se_3 nanosheets, time-dependent heating–cooling cycles under NIR laser were measured with 2 min laser heating and 10 min natural cooling (Fig. 4c). The cycles are repeated for five times and both of the two Bi_2Se_3 nanosheets exhibit excellent photostability.

3.4. Photoacoustic performance

When nanoparticles absorb external light, their raised temperature will induce a transient thermoelastic expansion,³⁶ which could launch ultrasonic waves to form photoacoustic images.³⁷ As a result, the photoacoustic signal of the nanoparticles heavily depends on its optical absorption ability and photoacoustic conversion efficiency, which represents the efficiency of the conversion of absorbed optical energy to acoustic waves.³⁸ Therefore, with the same optical absorption, the material with higher photoacoustic conversion efficiency is able to perform stronger photoacoustic signal.³⁹

Herein, the photoacoustic imaging is carried out to evaluate the photoacoustic conversion efficiency of the two Bi_2Se_3 nanosheets. Fig. 5 exhibits the photoacoustic images of the two Bi_2Se_3 nanosheets with same absorbance intensities of 0.3 at 808 nm. It is shown that the photoacoustic intensity of the Bi_2Se_3 -30 nanosheets is 3 times higher than the Bi_2Se_3 -80 nanosheets. Due to the smaller size of the Bi_2Se_3 -30 nanosheets, the increased temperature introduces more cavities and further promotes the thermoelastic expansion. Therefore, the more effective photothermal conversion and greater thermal expansion synergistically will result in the higher photoacoustic conversion capability of the Bi_2Se_3 -30 nanosheets.³⁸ Besides, the

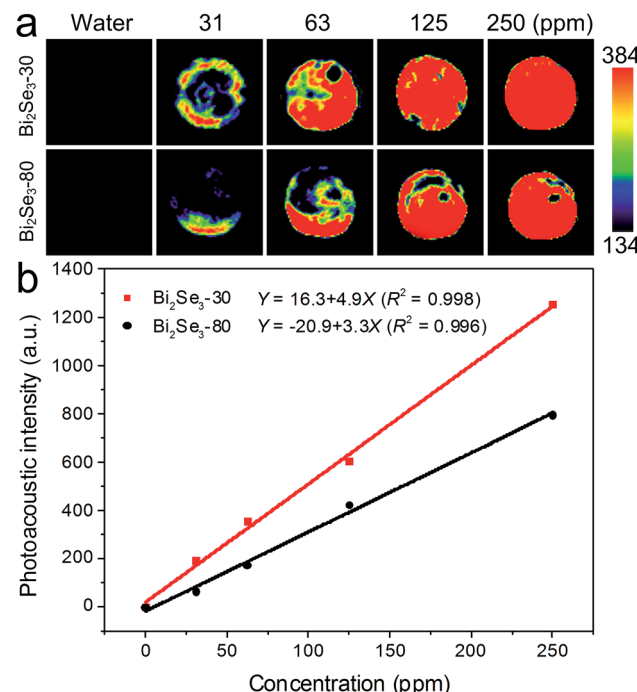


Fig. 6 (a) Photoacoustic images of the two Bi_2Se_3 nanosheets aqueous solution with different concentrations. (b) Photoacoustic signal intensities as function of the concentrations.

photoacoustic signal intensities of the two Bi_2Se_3 nanosheets are higher than that of GNRs, which is a commonly used photoacoustic agent (Fig. S4†).⁴⁰

Subsequently, the photoacoustic images of the aqueous solutions of the two Bi_2Se_3 nanosheets with concentrations from 0 to 250 ppm are illustrated in Fig. 6a. The concentration dependent intensities are described by the equations in Fig. 6b. The photoacoustic signals are enhanced with the increased Bi_2Se_3 concentrations. The Bi_2Se_3 -30 nanosheets show stronger photoacoustic signal than the Bi_2Se_3 -80 nanosheets at all concentrations, confirming their better NIR photoacoustic performance.

4. Conclusions

In this study, we have successfully prepared two Bi_2Se_3 nanosheets (Bi_2Se_3 -30 and Bi_2Se_3 -80) and characterized them utilizing TEM, HRTEM, XRD, EDS, AFM and UV-vis absorption spectroscopy. The results from optical absorption, NIR photothermal and photoacoustic effect demonstrate that both of the two Bi_2Se_3 nanosheets present excellent optical performances. In particular, the optical performances of Bi_2Se_3 -30 nanosheets with the smaller size are even better. These results indicate that the smaller Bi_2Se_3 nanosheets are more promising for optical diagnostic and photothermal therapy.

Conflicts of interest

There are no conflicts to declare.

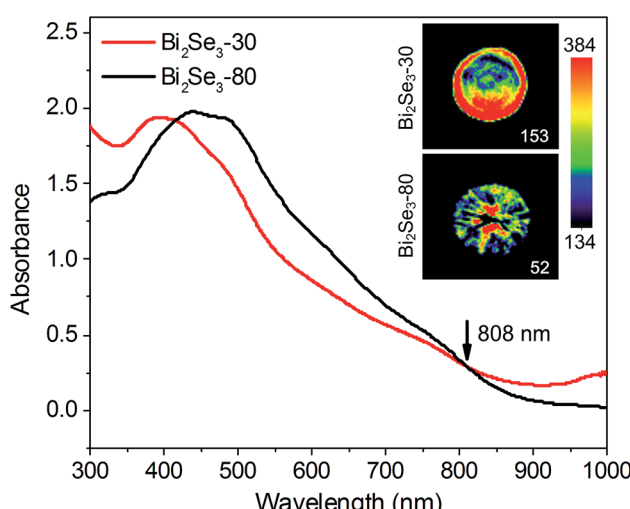


Fig. 5 Photoacoustic images of the two Bi_2Se_3 nanosheets with the same absorbance intensities of 0.3 at 808 nm.



Acknowledgements

This work was jointly supported by the National Natural Science Fund of China No. 51602204, Leading Talents of Guangdong Province Program (00201520), Guangdong Provincial Scientific Funds (2016A030313055), Program of Public Interest Research and Capability Construction of Guangdong Province (2015A020217010).

Notes and references

- 1 J. Moore, *Nat. Phys.*, 2009, **5**, 378.
- 2 D. Kong and Y. Cui, *Nat. Chem.*, 2011, **3**, 845.
- 3 Y. Xia, D. Qian, D. Hsieh, L. Wray, A. Pal, H. Lin, A. Bansil, D. Grauer, Y. S. Hor, R. J. Cava and M. Z. Hasan, *Nat. Phys.*, 2009, **5**, 398.
- 4 H. Peng, K. Lai, D. Kong, S. Meister, Y. Chen, X. Qi, S. Zhang, Z. Shen and Y. Cui, *Nat. Mater.*, 2010, **9**, 225.
- 5 H. Zhang, C. X. Liu, X. L. Qi, X. Dai, Z. Fang and S. C. Zhang, *Nat. Phys.*, 2009, **5**, 438.
- 6 Y. Min, J. W. Roh, H. Yang, M. Park, S. Kim, S. Hwang, S. M. Lee, K. H. Lee and U. Jeong, *Adv. Mater.*, 2013, **25**, 1425.
- 7 Y. L. Chen, J. G. Analytis, J. H. Chu, Z. K. Liu, S.-K. Mo, X. L. Qi, H. J. Zhang, D. H. Lu, X. Dai, Z. Fang, S. C. Zhang, I. R. Fisher, Z. Hussain and Z.-X. Shen, *Science*, 2009, **325**, 178.
- 8 K. Kadel, L. Kumari, W. Z. Li, J. Y. Huang and P. P. Provencio, *Nanoscale Res. Lett.*, 2011, **6**, 57.
- 9 L. Sun, Z. Lin, J. Peng, J. Weng, Y. Huang and Z. Luo, *Sci. Rep.*, 2014, **4**, 4794.
- 10 L. Cheng, S. Shen, S. Shi, Y. Yi, X. Wang, G. Song, K. Yang, G. Liu, T. E. Barnhart, W. Cai and Z. Liu, *Adv. Funct. Mater.*, 2016, **26**, 2185.
- 11 J. Li, F. Jiang, B. Yang, X. R. Song, Y. Liu, H. H. Yang, D. R. Cao, W. R. Shi and G. N. Chen, *Sci. Rep.*, 2013, **3**, 1998.
- 12 Z. Li, Y. Hu, K. A. Howard, T. Jiang, X. Fan, Z. Miao, Y. Sun, F. Besenbacher and M. Yu, *ACS Nano*, 2016, **10**, 984.
- 13 X. D. Zhang, J. Chen, Y. Min, G. B. Park, X. Shen, S. S. Song, Y. M. Sun, H. Wang, W. Long, J. Xie, K. Gao, L. Zhang, S. Fan, F. Fan and U. Jeong, *Adv. Funct. Mater.*, 2014, **24**, 1718.
- 14 B. L. Li, M. I. Setyawati, L. Chen, J. Xie, K. Ariga, C. T. Lim, S. Garaj and D. T. Leong, *ACS Appl. Mater. Interfaces*, 2017, **9**, 15286.
- 15 Y. Zhang, K. He, C. Z. Chang, C. L. Song, L. L. Wang, X. Chen, J. F. Jia, Z. Fang, X. Dai, W. Y. Shan, S. Q. Shen, Q. Niu, X. L. Qi, S. C. Zhang, X. C. Ma and Q. K. Xue, *Nat. Phys.*, 2010, **6**, 584.
- 16 J. Zhang, Z. Peng, A. Son, Y. Zhao, Y. Xiong, B. Peng, J. Wang, M. S. Dresselhaus and Q. Xiong, *Nano Lett.*, 2011, **11**, 2407.
- 17 Z. Li, S. Tang, B. Wang, Y. Li, H. Huang, H. Wang, P. Li, C. Li, P. K. Chu and X. F. Yu, *ACS Biomater. Sci. Eng.*, 2016, **2**, 789.
- 18 C. H. J. Choia, J. E. Zuckerman, P. Websterb and M. E. Davisa, *Proc. Natl. Acad. Sci. U. S. A.*, 2011, **108**, 6656.
- 19 Y. Min, G. D. Moon, B. S. Kim, B. Lim, J. S. Kim, C. Y. Kang and U. Jeong, *J. Am. Chem. Soc.*, 2012, **134**, 2872.
- 20 H. Xie, Z. Li, Z. Sun, J. Shao, X. F. Yu, Z. Guo, J. Wang, Q. Xiao, H. Wang, Q. Q. Wang, H. Zhang and P. K. Chu, *Small*, 2016, **12**, 4136.
- 21 Z. Li, J. Shao, Q. Luo, X. F. Yu, H. Xie, H. Fu, S. Tang, H. Wang, G. Han and P. K. Chu, *Biomaterials*, 2017, **133**, 37.
- 22 A. Zhuang, J. J. Li, Y. C. Wang, X. Wen, Y. Lin, B. Xiang, X. Wang and J. Zeng, *Angew. Chem.*, 2014, **126**, 6543.
- 23 S. Cho, N. P. Butch, J. Paglione and M. S. Fuhrer, *Nano Lett.*, 2011, **11**, 1925.
- 24 X. Liu, J. Xu, Z. Fang, L. Lin, Y. Qian, Y. Wang, C. Ye, C. Ma and J. Zeng, *Nano Res.*, 2015, **8**, 3612.
- 25 Z. Sun, S. Liufu, X. Chen and L. Chen, *Chem. Commun.*, 2010, **46**, 3101.
- 26 J. T. Robinson, S. M. Tabakman, Y. Liang, H. Wang, H. S. Casalongue, D. Vinh and H. Dai, *J. Am. Chem. Soc.*, 2011, **133**, 6825.
- 27 Y. Yi, X. F. Yu, W. Zhou, J. Wang and P. K. Chu, *Mater. Sci. Eng., R*, 2017, **120**, 1.
- 28 Z. Sun, H. Xie, S. Tang, X. F. Yu, Z. Guo, J. Shao, H. Zhang, H. Huang, H. Wang and P. K. Chu, *Angew. Chem.*, 2015, **127**, 11688.
- 29 L. Sun, Z. Lin, J. Peng, J. Weng, Y. Huang and Z. Luo, *Sci. Rep.*, 2014, **4**, 4794.
- 30 X. Yang, X. Wang and Z. Zhang, *J. Cryst. Growth*, 2005, **276**, 566.
- 31 S. Subramanian and P. Padiyan, *Mater. Chem. Phys.*, 2008, **107**, 392.
- 32 Q. Tian, F. Jiang, R. Zou, Q. Liu, Z. Chen, M. Zhu, S. Yang, J. Wang, J. Wang and J. Hu, *ACS Nano*, 2011, **5**, 9761.
- 33 J. Cui, R. Jiang, S. Xu, G. Hu and L. Wang, *Small*, 2015, **11**, 4183.
- 34 P. Huang, J. Lin, W. Li, P. Rong, Z. Wang, S. Wang, X. Wang, X. Sun, M. Aronova, G. Niu, R. D. Leapman, Z. Nie and X. Chen, *Angew. Chem.*, 2013, **125**, 14208.
- 35 C. M. Hessel, V. P. Pattani, M. Rasch, M. G. Panthani, B. Koo, J. W. Tunnell and B. A. Korgel, *Nano Lett.*, 2011, **11**, 2560.
- 36 L. Cavigli, M. Angelis, F. Ratto, P. Matteini, F. Rossi, S. Centi, F. Fusi and R. Pini, *J. Phys. Chem. C*, 2014, **118**, 16140.
- 37 L. V. Wang and S. Hu, *Science*, 2012, **335**, 1458.
- 38 Y. Shi, H. Qin, S. Yang and D. Xing, *Nano Res.*, 2016, **9**, 3644.
- 39 Y. S. Chen, W. Frey, S. Kim, P. Kruizinga, K. Homan and S. Emelianov, *Nano Lett.*, 2011, **11**, 348.
- 40 E. C. Cho, C. Kim, F. Zhou, C. M. Cobley, K. H. Song, J. Chen, Z. Y. Li, L. V. Wang and Y. Xia, *J. Phys. Chem. C*, 2009, **113**, 9023.

